Title
Manipulating the polarity of conductive polymer binders for Si-based anodes in lithium-ion batteries

Journal
Journal of Materials Chemistry A, 3(7)

ISSN
2050-7488

Authors
Wu, Mingyan
Song, Xiangyun
Liu, Xiaosong
et al.

Publication Date
2015

DOI
10.1039/c4ta06594h

Peer reviewed

Manipulating the polarity of conductive polymer binders for Si-based anodes in Lithium-ion Batteries

Mingyan Wu[1], Xiangyun Song[1], Xiaosong Liu[2], Vincent Battaglia[1], Wanli Yang[2], and Gao Liu[1]**

1. Environmental Energy Technologies Division, Lawrence Berkeley National Laboratory, Berkeley, CA 94720.
2. Advanced Light Source, Lawrence Berkeley National Laboratory, Berkeley, CA 94720.

KEYWORDS lithium-ion batteries, anode materials, Si, nanoparticle, polymer binder, conductive

ABSTRACT Si-based anodes continue to draw tremendous interest for lithium-ion batteries due to their large specific capacity for lithium. However, maintaining the stability while extracting high capacity from Si anodes stays a challenge because of significant volume changes during their electrochemical alloying and de-alloying with lithium. Polymer binder selection and optimization may allow dramatic improvements in the performance of Si-based anodes. Most studies of polymer binders of Si anodes have involved the use of insulating poly(vinylidene fluoride) (PVDF) and carboxyl group containing carboxymethylcellulose (CMC) or poly(acrylic acid) (PAA). Herein, we report for the first time the systematic studies on manipulating the polarity by adjusting the molar ratio of polar triethyleneoxide side chains, therefore the electrolyte up-taking properties changes systematically for conductive polyfluorene-based polymer binders. The results show that through optimizing the polarity of polymer binders, superior performance as a binder for Si anodes may be obtained. This study could be used as a model system and may open new avenues to explore a novel series of binders for both insulating and conductive polymer binder families.

INTRODUCTION

Lithium-ion batteries (LIBs) are one of the most promising next generation high density energy storage devices due to their numerous applications in information technology, electric vehicles, consumer electronic devices and the telecommunication industry.[1-4] Si has become an attractive anode materials because they are capable of delivering large specific capacity at 4200 mAh g^{-1}, far greater than the theoretical capacity of 372 mAh g^{-1} for graphite, which is the most commonly used anode material.[5] However, the practical applications of Si-based anodes have been inhibited by the stability issue arising from their huge volume expansion during alloying and de-alloying with lithium, leading to loss of electrical contact and fast electrode capacity fading.[6, 7]To accommodate this issue, much research has been focused on development of Si active materials (AM), mostly through nanostructured material design. In contrast, less attention has been devoted to the electrochemical inactive components of battery electrodes, such as binders. Binders are an important component of electrode formulation because they hold electrode particles together, maintain the physical structure of the electrode and further bond the AM particle based-electrode to its substrate-current collector. It has been gradually realized that many important battery characteristics, including stability and irreversible capacity losses, are critically dependent on the binders' selection and properties.[8-11] High-capacity electrochemically active particles, such as Si, in particular, that exhibit the largest volume changes during Li-ion battery operation, require further improved binder characteristics to ensure the physical integrity of electrodes during cycling.

In recent years, the new development of binders could be classified into two categories: (1) traditional poly(vinylidene fluoride) (PVDF) and carboxyl group containing carboxymethylcellulose (CMC) based polymer binders and their corresponding modified species or networks, [10, 12-17](2) electrical conductive polymer binders and/or conductive 3D networks.[11, 18-22] Earlier studies on PVDF binders for Si anodes have involved heat treatment of PVDF to different temperatures or using modified PVDF such as poly(vinylidene fluoride-tetrafluoroethylene-propylene) (PDVF-TFE-P) as binders.[12, 23]

The results indicated that the cycle stability of high capacity anode materials such as Si or Si-Sn alloy may benefit from the increased adhesion forces of PVDF by heat treatment or elasticity of the cross-linked binder system. Significant improvement of cycle performance was found using carboxyl group containing binders such as CMC, mixture of CMC-SBR[24], alginate[25], PAA[26], or 3D cross-linked networks between them[15]. This group of binders has high moduli, little-to-no interaction with electrolytes solvent, improved adhesion forces between carboxyl groups in binders and hydroxyl groups on Si surface. For example, charge-discharge between 0.01 and 1 V, the reversible Li extraction specific capacity of an alginate-based Si anode is in the range of 1700-2000 mAh g^{-1};[10] three-dimensionally cross-linked polymeric binder prepared by PAA and CMC exhibits a 2000 mAh g^{-1} after 100 cycles at 30 ºC.[15] However, relative high content of binder or conductive additives need to be added, which leads to a significant reduction in absolute anode capacity. In addition, further regulating the binder mechanical properties as well as swelling in an electrolyte solvent would be rather difficult due to their derivation from natural cellulose and polysaccharide. More recently, applying conductive polymer binders or conductive 3D networks for Si anodes has gain more popularity.[11, 18, 22] Due to the electrical conductivity of polymer binder itself, conductive additives such as acetylene black (AB), which has no binding force, become an unnecessary component of composited electrode. This not only potentially increases the electrode capacity but greatly helps to maintain the integrity and electrical conductivity of the high capacity Si electrode during LIB operation. For example, Lestriez et al presented a thick Si electrode with greatly improved cyclability based on a hierarchical and resilient conductive network carbon nanotubes and nanofibers;[27] a recent work from Cui's group reported that a well-connected 3D network structure consisting of Si

nanoparticles conformally coated by the *in-situ* polymerized conducting hydrogel. The resulting anodes were demonstrated a cycle life of 5,000 cycles with over 90% capacity retention at current density of 6.0□A□g^{-1}.[20] Our group recently developed a multi-functional polymer binder with high electronic conductivity, enhanced polarity, improved adhesion, ductility, and electrolyte uptake. Full-capacity cycling of Si nanoparticles was achieved by combination of developed polymer binder without adding any conductive additives.[11, 18]

However, for either conductive or nonconductive binders no such studies have been done on systematic investigation on the binder polarity effect on the cycle performance of Si-based anode for LIBs. Encouraged by our recent work, we herein report the follow-up work that four conductive polymer binders, which were purposely designed to have different polarity, were investigated and compared, to illustrate how the polarity of a conductive polymer binder plays a role on the cycle performance of Si-based anode for LIBs. The present findings may open up new prospects for the electrode performance optimization via better understanding the important role the binder and provide new guidelines for binder selection and electrode design.

EXPERIMENTAL SECTION

Raw Materials All the starting chemical materials for synthesis the conductive polymer were purchased from Sigma-Aldrich. Anhydrous N-methylpyrrolidone (NMP) with 50 ppm of water content was purchased from Aldrich Chemical Co. Silicon nanoparticles were purchased from Nanostructured & Amorphous Materials Inc. The particle sizes were below 100 nm in diameter. Lithium-ion electrolytes were purchased from BASF, including

1 M $LiPF_6$ in ethylene carbonate (EC) and diethylene carbonate (DEC) (1:1 w/w), 1 M $LiPF_6$ in EC and fluorinated ethylene carbonate (FEC) (7:3 w/w).

Synthesis PFM: A solution containing Poly(9,9-dioctylfluorene-co-fluorenone-co-methylbenzoic ester), mixture of 9,9-dioctylfluorene-2,7-diboronic acid bis(1,3-propanediol) ester (0.80 g, 1.43 mmol), 2,7-dibromo-9-fluorenone (0.24 g, 0.72 mmol), methyl 2,5-dibromobenzoate (0.21 g, 0.72 mmol), $(PPh_3)_4Pd(0)$ (0.082 g, 0.072 mmol), several drops of Aliquat 336, THF (13 mL) and 2 M Na_2CO_3 (5 mL) was refluxed at vigorous stirring for 72 h under an argon atmosphere. The solution was then concentrated by vacuum evaporation and the polymer was precipitated from methanol. The resulting polymer was further purified by precipitating from methanol twice. The final polymer was collected by suction filtration and dried under vacuum with a yield of 87%.1H NMR (400 M Hz, CDCl3) δ (ppm): 8.17 (s, Ar-H), 8.10 (s, Ar-H), 7.88 (m, Ar-H), 7.70 (m, Ar-H), 7.38-7.42 (d, Ar-H), 3.69 (s, OCH3), 2.10 (br, CH2), 1.2 (m, CH2), 0.8-0.9 (m, CH2, CH3). Anal. Calcd. for C19.95H23O0.71: C 87.40, H 8.46 Found: C 86.84, H 8.18. GPC (THF, PS standard): Mn = 36,000, PDI = 2.1.

Synthesis 2,7-Dibromo-9,9 (di(oxy-2,5,8-trioxadecane))fluorene 2,7-dibromofluorene (5.0 g, 15.4 mmol) was dissolved in dried THF solution (30 mL). Sodium hydride (1.0 g, 40 mmol) was added to the THF solution at room temperature and refluxed for five hours. 10-Tosyloxy-2,5,8-trioxadecane[28] (11.8 g, 37 mmol) in 20 mL of dry THF was added dropwisely to the refluxed solution. The mixture was allowed to reflux overnight, then cooled down, poured into distill water, and extracted with chloroform (2 × 100 mL). The combined organic solutions were washed with saturated NaCl solution (2

× 100 mL), distilled water (1 × 100 mL), dried over $MgSO_4$, and concentrated under reduced pressure. Crude oil was further purified by column chromatography to provide a 5.7 g product in 60% yield. 1H NMR (500 MHz, $CDCl_3$) δ (ppm): 2.34 (t, 4H), 2.77 (t, 4H), 3.10–3.60 (m, 22H), 7.40-7.60 (m, 6H).

Synthesis Poly(2,7-9,9-dioctylfluorene-co-2,7-9,9-(di(oxy-2,5,8-trioxadecane))fluorene-co-2,7-fluorenone-co-2,5-1-methylbenzoic ester) (PEFM): PEFM31, PEFM21, and PEFM41 were synthesized following same protocol with variation of relative molar ratio of monomers. For example, PEFM31was synthesized as follows: a mixture of 9,9-dioctylfluorene-2,7-diboronic acid bis(1,3-propanediol) ester (1.10 g, 1.97 mmol), 9,9-(di(oxy-2,5,8-trioxadecane))fluorine(0.44 g, 0.71 mmol) 2,7-dibromo-9-fluorenone (0.24 g, 0.72 mmol), methyl 2,5-dibromobenzoate (0.21 g, 0.72 mmol), $(PPh_3)_4Pd(0)$ (0.082 g, 0.072 mmol), and several drops of Aliquat 336 in a mixture of 13 mL of THF and 5 mL of 2 M Na_2CO_3 solution was refluxed with vigorous stirring for 72 hours under an argon atmosphere. The solution was then concentrated by vacuum evaporation, and the polymer was precipitated from methanol. The resulting polymer was further purified by precipitating from methanol twice. The final polymer was collected by suction filtration and dried under vacuum. 1H NMR (500 M Hz, $CDCl_3$) δ (ppm): 8.17 (s, Ar-H, 8.07 (s, Ar-H), 7.87 (m, Ar-H), 7.68 (m, Ar-H), 7.38-7.43 (d, Ar-H), 3.67 (s, OCH_3), 2.60-3.50 (m, -OCH_2CH_2O-), 2.10 (br, CH_2), 1.72 (br, CH_2), 1.17 (m, CH_2), 0.80-0.90 (m, CH_2, CH_3). GPC (THF, PS standard): Mn = 34,000, PDI = 2.3. For PEFM21, Mn = 17,955, PDI = 3.7; for PEFM41, Mn = 18,386, PDI=4.2.

Binder swelling test The compatibility of the binder with the electrolyte solvent was examined by the swelling test. Binder sheets were prepared by solution-cast samples and the solvents were removed under vacuum oven at 80 ºC. Binder sheets were then placed in ethylene carbonate (EC) and diethylene carbonate (DEC) (1:1 w/w) at room temperature. Weight measurements were made by blotting the samples dry and immediately weighting them. The swelling ratio was defined as the weight ratio of the amount of solvent absorbed to the dry weight of the tested binder sheet.

Electron Microscopy Composite electrode surface images were collected with a Hitachi S-4300SE/N scanning electron microscope (SEM) with an accelerating voltage of 15 kilovolts (kV) using the high vacuum mode at room temperature. High-resolution transmission electron microscope (HRTEM) images were obtained on a Philips CM200 field emission microscope operated at 200 kV at the National Center for Electron Microscopy (NCEM) at Lawrence Berkeley National Laboratory (LBNL).

Adhesion Test Adhesion measurements of the Si electrode were performed on a Chatillon® TCD225 series force measurement system. The Cu side of the Si electrode (1.2 cm × 1.2 cm) was fixed vertically to the bottom sample holder. The adhesive side of a 3M Scotch Magic® tape was applied onto the electrode laminate side firmly. The peel track was 1.2 cm wide. The Scotch Magic tape was peeled using the top sample holder at the direction of 180° angle to the adhered tape and parallel to one side of the Si electrode. The peeling speed was fixed at 7 min^{-1} moving rate to the bottom sample holder. The force applied to the adhered tape was recorded during the peeling process. When the tension

was fully applied and the electrode laminate was peeled off, the measured force value reaches a plateau, representing the adhesion force of the electrode laminates.

Contact Angle Measurements Experimental measurements of contact angles were performed with a custom-made automated goniometer (ramé-hart Model 590), which is capable of two-way injection and two-way image capturing as shown in our earlier work[11]. A charge-coupled device (CCD) camera (70 feet per second [fps]) of 640 × 480 pixels is utilized to capture images every quarter second, with a 150 W halogen lamp used as a backlight. The sample was first placed on the sample stage on top of a double-sided tape to avoid any displacement. A fixed volume of liquid water was then injected from above by a needle using an automated dispensing system with a constant injection rate. The sample-stage slowly raised until contact with the drop and slowly lowered as the drop was formed, to minimize any kinetic impact from the drop falling to the sample surface, which could produce erroneous measurements and add variability to the system. The optimum injection rate was determined using several measurements. For smaller drops, it was found that the contact-angle data were statistically consistent for the injection rate of 2 microliters per second (μL/s) or slower. However, in this study, we used a fixed drop volume of 10 μL and an injection speed of 0.5 μL/s for better accuracy. Movement of the stage was vibration-free, with no backlash, and vibrations from the surroundings were isolated from the stage using an anti-vibration stage. Several measurements were taken for each sample, while three contact-angle measurements were taken for each droplet with 1-second time interval using DROPimage® software.

X-ray Absorption Spectroscopy Synchrotron-based Carbon-*K* XAS Spectra were collected at beamline 8.0.1 of the Advanced Light Source at LBNL. The undulator and spherical grating monochromator supply a linearly polarized photon beam with resolving power up to 6000. Polymers were spin coated on clean gold (Au) surfaces then loaded into an experimental chamber with base pressure of about 8×10^{-10} torr. To avoid artificial effects from radiation damage, experiments were done at 85 K temperature with a deliberately defocused and low-flux x-ray beam. All the samples have been measured multiple times with different flux, scan period, and on different spots. Data have been carefully checked to make sure they are free of radiation damage effect. The XAS spectra shown here were collected in the total electron yield mode by registering the sample current normalized to the photon flux, which was measured simultaneously by the photocurrent of a clean Au mesh. The experimental resolution of the shown XAS spectra is better than 0.1 eV. All spectra plotted here were collected in one experiment with all samples mounted on the same holder to guarantee that the relative shift of the LUMO level is reliable.

RESULTS AND DISCUSSION

Scheme 1. Synthetic scheme and the relative molar ratio of four functional block of polymer binders.

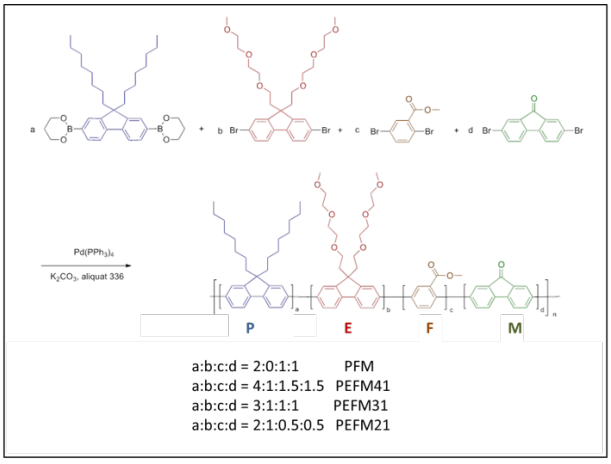

Scheme 1. shows the synthesis schematic of the conductive polymers under study, where P represents polyfluorene with octyl side chains, E represents triethyleneoxide monomethylether side chains, F represents fluorenone and M represents benzoate ester. The molar ratio among P, E, F and M was demonstrated by a, b, c, and d. In terms of their functionality, P contributes to the electric conductivity as polyfluorene type polymer block; E was introduced into the polymer to enhance its polarity, therefore its electrolyte uptake capability;[11] F was incorporated to tailor the electronic structure of the polymer, so the polymer could be cathodically doped under the reducing lithium environment to improve its overall electric conductivity;[11, 18] M groups were copolymerized to improve the chain flexibility of the polymer, and therefore strengthen the mechanical adhesion force between the active materials and the polymer binder. As shown in Scheme 1, the polarity of polymers, particularly, was designed from low to high by controlling the relative molar ratio between polymer block P and polymer block E with polar side chain from low to high, and they were named as PFM, PEFM41, PEFM31, and PEFM21, respectively.

Contact angle measurements were performed on spin-coated polymer films using liquid water as polar solvent. As shown in Table 1., the static contact angle of PFM, which was designed to

Table 1. Contact angle measurements of four polymers

Polymer	Contact Angle (degree)
PFM	97±1.0
PEFM41	96±1.5
PEFM31	89±1.0
PEFM21	88±1.0

have the lowest polarity, is the largest, around 97 degree. In contrast, the static contact angle of PEFM21, which was designed to have the highest polarity, is only about 88 degree, indicating

the much better water wetting with polymer films, confirming this polymer has higher polarity than that of PFM. The other two polymers contact angles fall in between which is consistent with the goal of design.

One advantage of our polymer system is the multi-functional groups that allow the tuning of individual functional group without detrimental to each other. We have previously established that introducing fluorenone (F) group into polyfluorene polymer allow lithium (Li) bonded to the polymer on the F group first, because the binding energy of Li to F group is 2.46 eV and is a bit higher than that of the Si (2.42 eV).[18] A special lowest unoccupied molecular orbital (LUMO) state derived from the F group sits lower in energy than that of the Li state. The electron distribution of this particular LUMO state is extended into the polymer backbone, leading to effective in-situ electron doping for improving the polymer's electric conductivity. Introducing E side chain does not contribute the relevant electronic state pertaining to the electronic conductivity, as confirmed by X-ray Absorption Spectroscopy (XAS) experiment. Figure 1 shows the synchrotron-based soft x-ray absorption spectroscopy (XAS) results, collected at the Advanced Light Source (ALS), Lawrence Berkeley National Laboratory (LBNL).

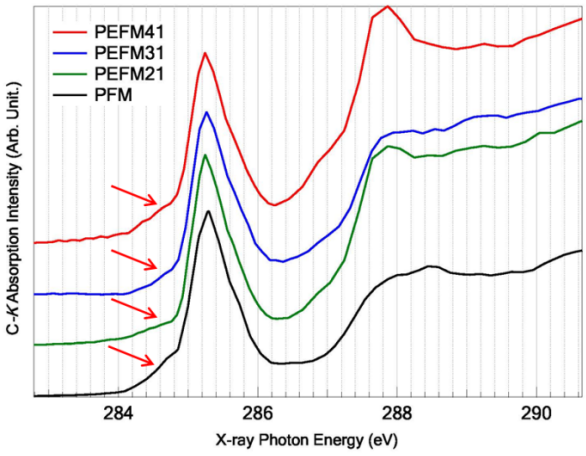

Figure 1. Synchrotron-based soft x-ray absorption spectra of a series of polymer binders with different polarity. Here we focus on low-energy onset states, which correspond to the LUMO-derived bands marked as arrows. E functional groups only affect high-energy features

The lowest energy of polymer binders marked by red arrows in XAS data corresponds to the LUMO states with empty core-holes. The results show clearly that a low-energy shoulder feature exists for all polymers with F groups, modifying the polar side chains E only leads to spectroscopic difference at higher energies away from the LUMO states, thus should have no effect on electrical conductivity.

Except the inherent electrical conductivity in reducing environment of lithium-ion battery operation, an ideal polymer binder should provide excellent mechanical adhesion forces between AM particles and current collector. Adhesion forces of composited electrodes based on four polymer binders were evaluated by peel tests. The weight ratio of Si NPs was kept same level as 67% and polymer binder weight ratio was 33%. The loading of Si NPs was about 0.3 mg cm^{-2}. As shown in Figure 2, Si electrodes based on PEFM31 and PEFM41 exhibit the highest load

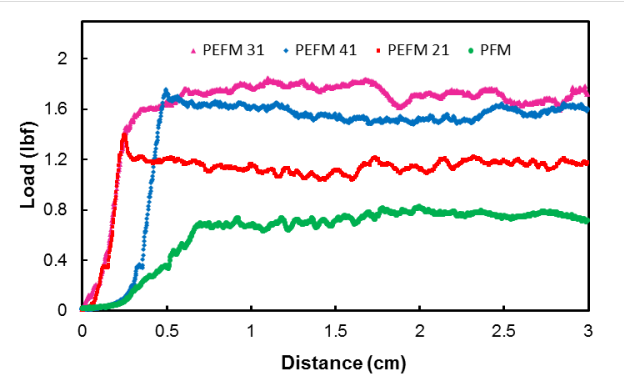

Figure 2. Force measured during the peel tests of PFM and PEFM21, PEFM31, PEFM41 based electrodes.

forces at about 1.7 lbf, and the plateau of PEFM41 is slightly below PEFM31. The load force of PEFM21 reduced significantly to 1.2 lbf, and PFM shows the smallest load force at only 0.8 lbf. It should be noted that the load forces for PEFM31 and PEFM41 are the forces to partially peel off the laminate from current collector, and majority of laminate persists on the current collector; in contrast, the load forces for PEFM21 and PFM are the forces that peel off the whole laminate from current collector, as shown in our earlier work.[11] As the binders' polarity increases, the binder adheres with the polar silicon dioxide (SiO_2) surfaces of the Si particle and the copper oxide (CuO) surface of the Cu current collector more effectively.[26] However, too much polar E group decreases mechanical properties of the binder by making it a too soft polymer material, and when used as a binder, its adhesion force goes down.

In addition, Li-ion transportation efficiency at the interface between polymer binder and active materials is critical for extracting the full capacity of active materials because polymer coating on the surface of active materials may block the Li-ion diffusion to active materials. Although ion mobility in the doped conductive polymer system has been demonstrated, strategies to further improve the ion mobility are still necessary[29, 30]. In our system, manipulating the polarity, therefore the swellability of polymer binders provides the direct way to optimize the Li-ion transportation efficiency of polymer binders. We measured the swellability of the polymer films in ethylene carbonate (EC) and diethylene carbonate (DEC) (1:1 w/w) at room temperature. Swelling ratio is defined as weight increase ratio by adsorbed solvent to the weight of the dry polymer films. As shown in Figure 3, PFM has electrolyte uptake only up to 10 percent of its dry

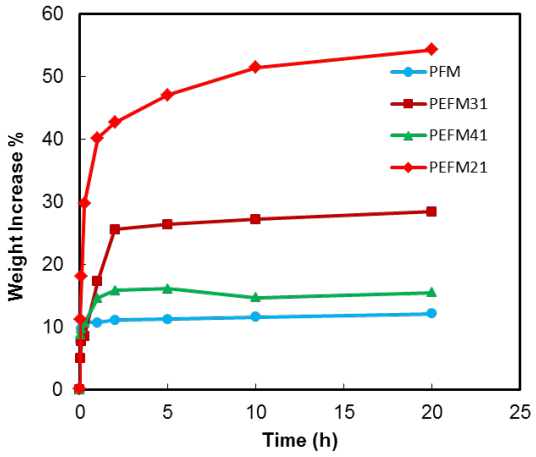

Figure 3. The swelling tests of polymer films in the EC/DEC (1:1) electrolyte.

state in 20 hrs, whereas PEFM41 shows a bit higher electrolyte uptake about 15 percent, PEFM31 almost triple the electrolyte uptake compared to that of PFM, reaches around 28 percent. It should be noted that 28 percent swelling recalls the non-conductive polymer and shows similar swelling ability as popular binder PVDF.[13] Last but not least, the polymer binder PEFM21, which has the highest polarity in this system shows electrolyte uptake exceeds 50 percent. As can been seen, the trend of the swelling of four polymer binders is consistent with the trend of water contact angle measurements. (Table 1), indicating the chemically attached ether side groups in the binder help to improve the overall electrolyte uptake significantly. Li-ion transport is fast in EC/DEC based liquid electrolyte. Increasing the swellability of the polymer binder increases electrolyte penetration into the polymer binder, therefore enhances Li-ion transport in the electrode. This also decreases interfacial impedance between Si and polymer binders. Higher swellability of polymer binders also suggests it should behave as a more deformable material. As mentioned earlier, for high-capacity electrodes such as Si, a more complaint polymer binder is highly desirable because the higher scale of volume expansion occurs in Si electrodes. The volume expansion causes the accumulative stress which leads to the fracture of the electrode. This fracture takes place within the binder itself, and/or

at the binder/Si interface, but not in the Si particles. Most of the conductive polymers, however, are rigid molecules that tend to have higher Young's modulus (elastic modulus) and are very brittle[31]. Conversely, in our conductive polymer binder system, for the first time, the elasticity of the conductive polymer binder was systemically manipulated in molecular level by introducing polar ether moieties. The more compliant binders should better accommodate the volume change of active materials, and they accumulate less stress in the binder and at the interface between the binder and the active materials. This model PEFM binder system could be used to study how the polarity of conductive polymer binder affects the performance of Si anodes. This study may also provide guidelines for nonconductive binders, such as CMC/PAA based binders, as systematic investigation has not been done on the impact of binder elasticity on functional binders.

The electrochemical performance of four polymer binders with different polarity was shown in Figure 4.For better comparison, all cells under testing were made of cells using Li metal as the counter electrode. As seen in Figure 4, all the polymer binder based electrodes have the similar

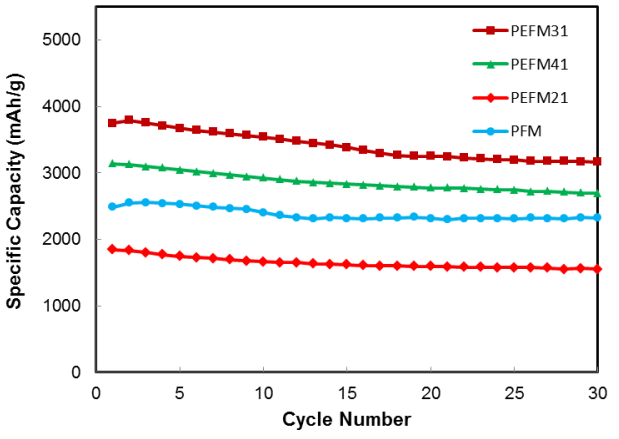

Figure 4. Cycling performance of polymer/Si electrodes without any conductive additive.

trend for the cycling performance, that is, they are observed faster fading at the first 10 cycles and become more stabilized at extended 30 cycles. However, the charge capacity (delithiation) of these polymer binders differs from each other. More specifically, the polymer binder with medium polarity, PEFM31, achieved the highest charge capacity 3750 mAh g^{-1} at the initial cycles, reaching the full achievable theoretical capacity of Si materials. The observed capacity is more than 1000 mAh g^{-1} higher than that of PFM, which does not contain polar E group. PEFM41, which has less polarity than PEFM31, but higher polarity than PFM, shows the 2nd highest capacity at 3000 mAh g^{-1}. PEFM21, the polymer binder having the highest polarity, however, is observed the capacity less than 2000 mAh g^{-1}, and this value is even lower than that of the polymer binder PFM without introducing the polar E moieties.

Rate performance of four polymer binder based electrodes was investigated using constant discharge (lithiation) rate at C/25 and various charge (delithiation) rate. Although these four polymer based electrodes differ dramatically in charge capacity, they exhibit similar descending trend when charge rate increases from C/25 to 2 C, as shown in figure 5. Particularly for

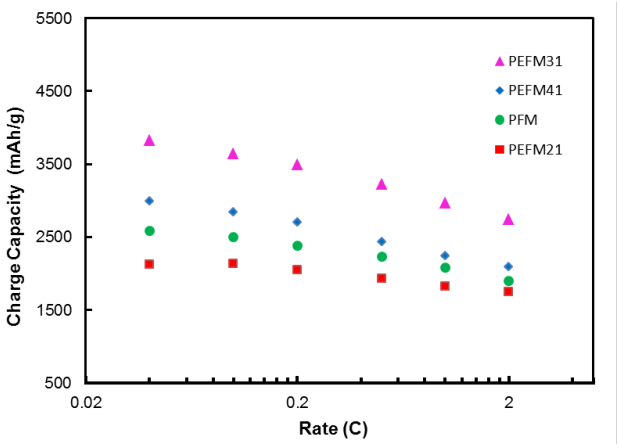

Figure 5. The rate performance of the polymer/Si electrodes with four polymer binders at various charge rates. Discharge rate was kept at C/25.

PEFM31, it reaches full theoretical capacity at C/10 rate and still maintains much higher capacity at 2 C compared to other polymer based electrodes, and the retention is over 70% at this high rate. The retention of PEFM21 is slightly higher than PEFM31 at 2 C, however, when considering its charge capacity is only half of PEFM31, the rate capability does not improve significantly.

More information comes from the post-analysis of the electrodes after cycling. PEFM31 and PEFM21 were selected to show distinct difference as they exhibit the largest difference in specific capacity. As shown in Figure 6, the fresh composite electrodes of PEFM31/Si and PEFM21/Si share similar morphology with polymer binder coating on the surface of Si NPs (Figure 6 a, d). After one cycle of lithiation and delithiation, in TEM image, Si NPs still could be seen embedding within polymer matrix for both polymer binders (Figure 6 b, e). However, the electron diffraction pattern shows complete amorphous feature for PEFM31/Si (Figure 6 c); in

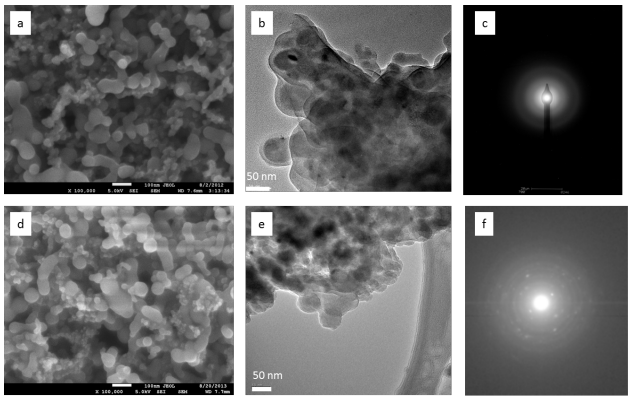

Figure 6. Electron microscope images polymer/Si electrodes before and after cycling. (a) SEM of a fresh composite electrode with conductive polymer binder PEFM31 and Si nanoparticles. (b) TEM image of PEFM31/Si composite electrode after one lithiation and delithiation cycle. Si can been seen embedded within polymer matrix. (c) The electron diffraction pattern of PEFM31/Si composite electrode indicates completely amorphous Si particle in the composite electrode. (d)

SEM of a fresh composite electrode with conductive polymer binder PEFM21 and Si nanoparticles. (e) TEM image of PEFM21/Si composite electrode after one lithiation and delithiation cycle. Si can been seen embedded within polymer matrix. (f) The electron diffraction pattern of PEFM31/Si composite electrode. The diffraction spots suggest the existence of crystalline Si particles.

contrast, the diffraction pattern of PEFM21/Si shows the obvious existence of crystalline Si domain (Figure 6 f). This result is consistent with the electrochemical performance of these two composited electrodes (Figure 4), indicating the full accessibility of Li-ion diffusion to Si active materials through the interface between the polymer binder PEFM31 and Si. The excessively swelling of PEFM21, although facilitates lithium ion transport within the binder, increases electronic resistance of the conductive polymer binder. The increased electron impedance partially isolates Si particles from the electrical network, preventing Si from participating in electrochemical lithiation and delithiation.

As we established before, the superior performance of PEFM31 comes from the optimum polarity of PEFM31 binders, compared to that of the other two polymer binders with low E content (PEFM41) and with no E content (PFM) .[11] However, further increasing the polarity of polymer binder to PEFM21 lead to excessive swelling, causing detrimental effect on the electrochemical performance of the PEFM21/Si electrodes.

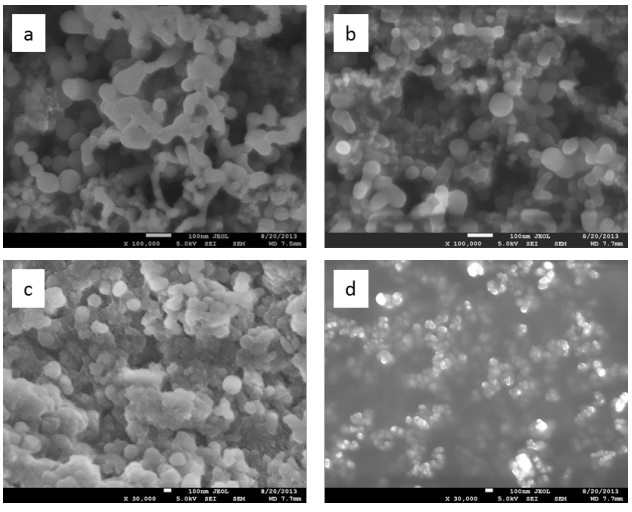

Figure 7. Electron microscope images polymer/Si electrodes before and after cycling. (a) SEM of a fresh composite electrode with conductive polymer binder PFM and Si NPs. (b) SEM of a fresh composite electrode with conductive polymer binder PEFM21 and Si NPs. (c) SEM image of PEFM41/Si electrode after one lithiation and delithiation cycles. (d) SEM image of PEFM21/Si electrode after one lithiation and delithiation cycles.

To better understanding this behavior, careful comparison between SEM images after one lithiation and delithiation cycle was also performed. Figure 7 shows the SEM images of composited electrodes made of PEFM41 and PEFM21 polymer binder, which have large difference in polarity. As mentioned earlier, the fresh electrodes of these two polymer binders also show similar morphology (Figure 7 a, b). After 1 cycle of lithiation and delithiation, Si NPs can be clearly seen and pores are still observed for PEFM41/Si electrode (Figure 7 c). In contrast, the SEM image of PEFM21/Si becomes more blurred, and Si NPs are embedded within a thick layer of a polymer matrix and pores are mostly covered up. Considering the polymer binder weight ratio was kept same for all electrodes. The movement of polymer binder is the main cause of the morphological evolution of the electrode surfaces. The polymer binders are squeezed to the surface of electrode during cycling due to the volume expansion of Si particles. Although both PEFM41 and PEFM21 base electrode show less porosity on the surface of electrode after cycling, the high swelling rate of PEFM21 make it easy for PEFM21 binder to move up to the surface. Moreover, the high swelling of PEFM21 tends to trap more electrolyte in the electrode, causing decomposition of electrolyte at the Si surface. The decomposition product accumulate on the surface of Si NPs during lithiation and delithiation process, which covers the pores of the electrode and block the efficient Li-ion diffusion to Si active materials.[26]

CONLUSION

In summary, by exclusively manipulating the polarity of conductive polymer binders, the effect of polymer binder polarity, therefore the electrolyte uptake properties on the electrochemical performance of Si based anodes is illustrated. The results show polarity of polymer binder plays an important role for the electrode performance, and optimized binder

selection and design may lead to superior performance of the electrodes. These findings could be used as a model system and may open new avenues to explore a novel series of binders from both insulating and conductive polymer binder families.

Corresponding Author

* Gao Liu Gliu@lbl.gov

Author Contributions

M.W. V.B. and G.L. conceived the experiments. M.W. performed material synthesis, characterization and electrochemical testing. X.S. performed TEM analysis. X. L. and W.Y. carried out the soft X-ray spectroscopy analysis. G. L. directed the research. M.W., W.Y and G.L. wrote the paper.

ACKNOWLEDGMENT

This work is funded by the Assistant Secretary for Energy Efficiency, Office of Vehicle Technologies of the U.S. Department of Energy, under the Batteries for Advanced Transportation Technologies (BATT) Program and by University of California, Office of the President through the University of California Discovery Grant. Soft x-ray Spectroscopy was performed at the Advanced Light Source (ALS). Electron microscopy experiments were conducted at the National Center for Electron Microscopy (NCEM). NMR spectroscopy experiments were performed at the Molecular Foundry. All facilities are located at Lawrence Berkeley National Laboratory (LBNL), and are supported by the Director, Office of Science, Office of Basic Energy Sciences, of the US Department of Energy under contract no. DE-AC02-05CH11231.

REFERENCES

(1) Tarascon, J. M.; Armand, M. *Nature* **2001,** *414*, 359-367.
(2) Armand, M.; Tarascon, J. M. *Nature* **2008,** *451*, 652-657.
(3) Whittingham, M. S. *Mrs. Bull.* **2008,** *33*, 411-419.
(4) Kang, B.; Ceder, G. *Nature* **2009,** *458*, 190-193.
(5) Li, J.; Dahn, J. R. *J. Electrochem. Soc.* **2007,** *154*, A156-A161.
(6) Christensen, J.; Newman, J. *J. Electrochem. Soc.* **2006,** *153*, A1019-A1030.
(7) Renganathan, S.; Sikha, G.; Santhanagopalan, S.; White, R. E. *J. Electrochem. Soc.* **2010,** *157*, A155-A163.
(8) Bridel, J. S.; Azaïs, T.; Morcrette, M.; Tarascon, J. M.; Larcher, D. *Chem. Mater.* **2009,** *22*, 1229-1241.
(9) Guo, J.; Wang, C. *Chem. Commun.* **2010,** *46*, 1428-1430.
(10) Kovalenko, I.; Zdyrko, B.; Magasinski, A.; Hertzberg, B.; Milicev, Z.; Burtovyy, R.; Luzinov, I.; Yushin, G. *Science* **2011,** *334*, 75-79.
(11) Wu, M.; Xiao, X.; Vukmirovic, N.; Xun, S.; Das, P. K.; Song, X.; Olalde-Velasco, P.; Wang, D.; Weber, A. Z.; Wang, L.-W.; Battaglia, V. S.; Yang, W.; Liu, G. *J. Am. Chem. Soc.* **2013,** *135*, 12048-12056.
(12) Chen, Z. H.; Christensen, L.; Dahn, J. R. *J. Electrochem. Soc.* **2003,** *150*, A1073-A1078.
(13) Liu, W.-R.; Yang, M.-H.; Wu, H.-C.; Chiao, S. M.; Wu, N.-L. *Electrochemical and Solid-State Letters* **2005,** *8*, A100-A103.
(14) Li, J.; Lewis, R. B.; Dahn, J. R. *Electrochem. Solid St* **2007,** *10*, A17-A20.
(15) Koo, B.; Kim, H.; Cho, Y.; Lee, K. T.; Choi, N. S.; Cho, J. *Angew. Chem. Int. Edit.* **2012,** *51*, 8762-8767.
(16) Han, Z. J.; Yabuuchi, N.; Hashimoto, S.; Sasaki, T.; Komaba, S. *Ecs Electrochemistry Letters* **2013,** *2*, A17-A20.
(17) Ryou, M. H.; Kim, J.; Lee, I.; Kim, S.; Jeong, Y. K.; Hong, S.; Ryu, J. H.; Kim, T. S.; Park, J. K.; Lee, H.; Choi, J. W. *Adv. Mater.* **2013,** *25*, 1571-6.
(18) Liu, G.; Xun, S. D.; Vukmirovic, N.; Song, X. Y.; Olalde-Velasco, P.; Zheng, H. H.; Battaglia, V. S.; Wang, L. W.; Yang, W. L. *Adv. Mater.* **2011,** *23*, 4679-4683.
(19) Joyce, C.; Trahey, L.; Bauer, S. A.; Dogan, F.; Vaughey, J. T. *J. Electrochem. Soc.* **2012,** *159*, A909-A914.
(20) Wu, H.; Yu, G.; Pan, L.; Liu, N.; McDowell, M. T.; Bao, Z.; Cui, Y. *Nat Commun* **2013,** *4, 1943-1952*.
(21) Thakur, M.; Pernites, R. B.; Nitta, N.; Isaacson, M.; Sinsabaugh, S. L.; Wong, M. S.; Biswal, S. L. *Chem. Mater.* **2012,** *24*, 2998-3003.
(22) Wu, M.; Sabisch, J. E. C.; Song, X.; Minor, A. M.; Battaglia, V. S.; Liu, G. *Nano Lett.* **2013,** *13*, 5397-5402.
(23) Li, J.; Christensen, L.; Obrovac, M. N.; Hewitt, K. C.; Dahn, J. R. *J. Electrochem. Soc.* **2008,** *155*, A234-A238.
(24) Liu, W.; Yang, M.; Wu, H.; Chiao, S. M.; Wu, N. *Electrochem. Solid St* **2005,** *8*, A100-A103.
(25) Kovalenko, I.; Zdyrko, B.; Magasinski, A.; Hertzberg, B.; Milicev, Z.; Burtovyy, R.; Luzinov, I.; Yushin, G. *Science* **2011,** *334*, 75-79.
(26) Magasinski, A.; Zdyrko, B.; Kovalenko, I.; Hertzberg, B.; Burtovyy, R.; Huebner, C. F.; Fuller, T. F.; Luzinov, I.; Yushin, G. *ACS Appl Mater Inter* **2010,** *2*, 3004-3010.
(27) Lestriez, B.; Desaever, S.; Danet, J.; Moreau, P.; Plée, D.; Guyomard, D. *Electrochemical and Solid-State Letters* **2009,** *12*, A76-A80.
(28) Liu, G.; Baker, G. L. *Soft Matter* **2008,** *4*, 1094-1101.
(29) Jow, T. R.; Shacklette, L. W. *J. Electrochem. Soc.* **1988,** *135*, , 541-548.
(30) Pei, Q. B.; Yang, Y. *J. Am. Chem. Soc.* **1996,** *118*, 7416-7417.

(31) Hu, X. D., Jenkins, S. E., Min, B. G., Polk, M. B. & Kumar, S. *Macromol. Mater. Eng.* **2003,** *288*, 823-843.

For Table of Content only

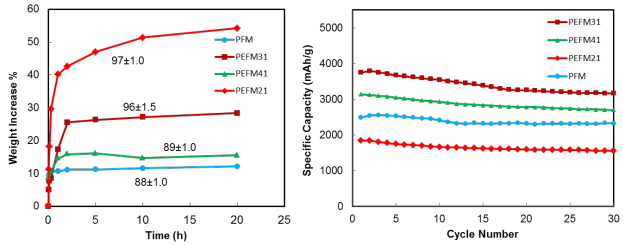
Weight Increase %
Time (h)
PFM
PEFM31
PEFM41
PEFM21
97±1.0
96±1.5
89±1.0
88±1.0
Specific Capacity (mAh/g)
Cycle Number